Radiology. Author manuscript; available in PMC 2017 August 01.

Published in final edited form as:

Radiology. 2017 August ; 284(2): 451–459. doi:10.1148/radiol.2017161687.

Luminal Water Imaging: a New MRI T_2 Mapping Technique for Prostate Cancer Diagnosis

Shirin Sabouri, MSc[1], **Silvia D. Chang, MD**[2,4,6], **Richard Savdie, MD**[4], **Jing Zhang, PhD**[3], **Edward C. Jones, MD**[5], **S. Larry Goldenberg, MD**[4,6], **Peter C. Black, MD**[4,6], and **Piotr Kozlowski, PhD**[2,3,4,6]

[1]Department of Physics and Astronomy, University of British Columbia, Vancouver, BC, Canada

[2]Department of Radiology, University of British Columbia, Vancouver, BC, Canada

[3]UBC MRI Research Center, Vancouver, BC, Canada

[4]Department of Urologic Sciences, University of British Columbia, Vancouver, BC, Canada

[5]Department of Pathology and Laboratory Medicine, University of British Columbia, Vancouver, BC, Canada

[6]Vancouver Prostate Centre, Vancouver, BC, Canada

Abstract

Purpose—To assess the feasibility of luminal water imaging (LWI), a quantitative T_2-based MRI technique, for the detection and grading of prostatic cancer (PCa).

Material and Methods—18 patients with biopsy proven PCa provided informed consent to be included in this institutional human ethics board approved prospective study between January 2015, and January 2016. Patients underwent 3T MRI shortly before radical prostatectomy. T_2 distributions were generated with regularized Non-Negative Least Squares (NNLS)algorithm from multi-echo spin echo MRI data. From T_2 distributions, maps of seven MR parameters: N_{comp}, $T_{2\text{-short}}$, $T_{2\text{-long}}$, geometric mean T_2 (gmT_2), Luminal Water Fraction (LWF), A_{short}, and A_{long} were generated and compared with digitized images of Hematoxylin and Eosin (H&E) stained whole-mount histology sections. Paired-t-test determined significant differences between MR parameters in malignant and non-malignant tissue. Correlation with Gleason score (GS) was evaluated with Spearman's rank correlation test. Diagnostic accuracy was evaluated using logistic generalized linear mixed effect models (GLMMs) and receiver operating characteristic (ROC) analysis.

Results—The average values of four MR parameters: gmT_2, A_{short}, A_{long}, and LWF were significantly different between malignant and non-malignant tissue. All MR parameters except for $T_{2\text{-long}}$ showed significant correlation ($P<0.05$) with GS in peripheral zone (PZ). The highest correlation with GS was obtained for LWF (-0.78 ± 0.11, $p < 0.001$). The results of ROC analysis

Contact information of the corresponding author: Shirin Sabouri, Telephone number: +1 604-827 3972, Fax number: +1 604-827 3973, sabouri@phas.ubc.ca.

Institution:
The University of British Columbia, 2329 West Mall, Vancouver, BC, Canada, V6T 1Z4

demonstrated high accuracy of tumour detection, with the highest value of area under the ROC curve (AUC) obtained for LWF (0.97 in PZ and 0.98 in TZ).

Conclusion—Results of this pilot study demonstrate the feasibility of LWI to detect and grade prostate cancer. A study with larger cohort of patients and broader range of GS is required to further evaluate this new technique in clinical settings.

Introduction

Magnetic resonance (MR) quantitative T_2 mapping is a well-known imaging technique that has been used for tracking histopathologic changes in brain [1] and cartilage [2]. In this technique, a series of MR T_2-weighted spin-echo images are acquired, from which a signal decay curve can be generated and T_2 relaxation time determined for each pixel. In homogenous systems, T_2 relaxation process is mono-exponential with a well-defined T_2 relaxation time. However, in inhomogeneous tissues, where each voxel contains various water compartments, the signal decay curve becomes multi-exponential, with several different T_2 relaxation times.

Multiple T_2 values reflect underlying composition of the scanned tissue, and hence their measurement can reveal important information for diagnostic purposes. Prostatic tissue is composed of water compartments of different sizes, whose relative percentages vary between tumor and normal tissue [3], and between different pathologic grades of cancer. The glandular tissue of normal prostate is composed of stromal tissue fused to several ducts and acini, which consist of a lumen space filled with prostatic fluid and lined with two layers of epithelial cells [4, 5]. In such tissue, two distinctive water environments are expected, the larger one being the lumen space, and the much smaller intra-/extra-cellular space of epithelial and stromal tissue. Therefore, T_2 decay curves will likely be bi-exponential, with longer T_2 related to the water inside the lumen and a shorter T_2 to the water within the epithelial cells and stromal tissue.

Evidence of bi-exponential T_2 decay in prostate has previously been shown [6, 7, 8, 9], and recently investigated for potential contribution to prostate cancer diagnosis [10]. In this study, we investigated the relationship between multi-exponential T_2 mapping and the histopathology of prostatic tissue through a direct comparison between MRI and whole-mount histology. We introduce here a new parameter called luminal water fraction (LWF), which represents the fractional volume of the luminal space. Because of the difference in composition and lumen percentage between normal and cancerous tissues, we hypothesize that LWF could be used for the detection of prostate cancer. Moreover, since the relative amount of lumen decreases with the advancing Gleason score (GS), we also hypothesize that LWF could correlate to prostate cancer grading. The purpose of this study was to investigate the feasibility of this technique in the detection and grading of prostate tumors.

Materials and Methods

Patient Selection

This was an institutional human ethics board approved prospective study. Eighteen patients (median age, 65.5 years; age range 58–80.3 years) were recruited consecutively during

January 2015 to January 2016. These were patients referred to the Vancouver General Hospital Urology Clinic and diagnosed with prostate cancer. Additional inclusion criteria included patients: with biopsy-proven prostatic adenocarcinoma, no prior treatment, no contraindications to MRI, able to tolerate the endorectal coil and scheduled for radical retropubic prostatectomy. All patients gave informed signed consent prior to undergoing MRI examination shortly before surgery (median 11 days, range 1–41 days).

MR Imaging Protocol

MRI examinations were carried out on a 3T MRI scanner [Philips Medical Systems, Best, The Netherlands]. MR signals were acquired with a combined endorectal/pelvic phased-array coils (Medrad, Pittsburgh, PA, USA). Angled axial images were obtained in the plane perpendicular to the rectal wall-prostate interface, with a 3D multi-echo spin echo sequence developed at the University of British Columbia MRI Research Centre [12] (TR=3073 msec, TE=25 msec, NE=64, FOV=240×240×56mm^3, voxel-size=1×1×4mm^3, scan matrix-size=240×119, reconstruction matrix-size=240x240, slice thickness=4mm, flip angle=90°, number of averages=1, sense factor= 1.5, scan duration=673 sec). Values of the pulse sequence parameters were optimized through simulations to maximize the accuracy of T_2 measurements in prostate.

High spatial resolution T_2-weighted MR images were acquired with the same orientation, slice thickness, and slice location, by using a multi-slice Turbo Spin Echo (TSE) sequence (TR=1851 msec, effective TE = 80 msec, NE = 1, FOV=140×140×72mm^3, voxel-size=0.3×0.3×4mm^3, scan matrix-size=288×228, reconstruction matrix-size=512×512, slice thickness=4mm, flip angle=90°, number of averages=3, scan duration=285 sec). The number and positioning of the slices was set to cover the entire prostate.

Histologic examination and matching to MR images

Following prostatectomy, the excised specimens were immersed in 10% buffered formalin for a minimum of 48 hours. The formalin-fixed specimens were dissected and examined histopathologically in a uniform and consistent manner. The external surfaces were inked and the seminal vesicles and vas deferens amputated. The apical and bladder neck tissue were each removed as 0.5 cm thick tissue doughnuts. The complete prostate gland was then cut perpendicularly to the posterior surface of the prostate into 4 mm transverse slices with a multi-blade cutting device, developed in-house [11]. These Hematoxylin and Eosin (H&E) stained whole-mount slides were histologically examined by a genitourinary pathologist (E.C.J with 30 years' experience), who outlined the tumors and assigned the Gleason scores on each slide under the light microscope.

The whole-mount histology sections, digitized using a flatbed scanner, were registered to MR images with a software package developed in-house [13] using Matlab (The Math Works Inc., Natick, MA, USA). As described previously [13], the multi-step process involved registration of histology sections and high resolution T2-weighted and multi-echo images. This process resulted in deforming the original manually drawn (by consensus (S.S, S.D.C with 15 years experience in prostate MRI) ROIs, rather than MRI images, and thus

the ROI averages were calculated from non-deformed parametric maps, ensuring their accuracy.

Data Processing

All MR data were processed offline with software developed in-house using Matlab. Signal decay curves were fitted to multi-exponential function using regularized Non-Negative Least Squares (NNLS) [14, 15] algorithm. The fitting performed for each pixel of each slice resulted in smooth T_2 distributions (Figure 1). Similar to the analysis of multi-echo data acquired with Myelin Water Imaging in the brain [16, 17], the following parameters were defined to characterize T_2 distributions, $S(T_2)$: number of distinguishable T_2 components (N_{comp}); geometric mean of the short ($T_{2\text{-short}}$) and long ($T_{2\text{-long}}$) components, and the geometric mean of the entire distribution (gmT_2); ratio of the area under the long component over the area under the entire distribution (LWF); and areas under the short (A_{short}) and long (A_{long}) components. N_{comp} was obtained by counting the number of peaks in the distribution (See Figure 1). gmT_2 was calculated as explained previously in Ref. [14] by summing $S(T_2) \times \log(T_2)$ within the entire distribution (20 – 2000 msec) and dividing by the sum of all $S(T_2)$ within the entire distribution. $T_{2\text{-short}}$ and $T_{2\text{-long}}$ were calculated similar to gmT_2 except that their related summations were calculated within the distribution region of first peak (20–200 msec) and second peak (200–2000 msec), respectively. LWF was defined similar to the area fraction described by Bjarnason and Mitchell [14] and was calculated by summing $S(T_2)$ within the distribution region of the second peak and dividing by the sum of all $S(T_2)$ within the entire distribution. A_{short} and A_{long} were calculated by summing $S(T_2)$ within the distribution region of first peak and second peak, respectively.

Maps of these parameters were generated for every slice. Average values of MR parameters were calculated within a total of 378 (226 non-malignant, and 152 malignant) ROIs manually outlined on the registered whole-mount histology images in malignant peripheral (PZ) and transition (TZ) zones, non-malignant PZ and TZ, normal Anterior Fibromuscular Stroma (AFM), and Periurethral Fibromuscular Stroma (PFMS). Malignant ROIs were selected by accurately outlining the tumor boundaries delineated by pathologist. Non-malignant ROIs were selected by avoiding the tumor boundaries. Since regions of benign prostatic hyperplasia (BPH) were not outlined by pathologist, non-malignant ROIs in TZ could consist of BPH.

Statistical Analysis

Statistical analyses were performed using MedCalc (MedCalc Software, Mariakerke, Belgium) and R packages [18, 19, 20]. None of the MR parameters were normally distributed, as confirmed by the Kolmogorov-Smirnov test. Significant differences between malignant and non-malignant tissues were determined with paired t-test. In order to account for the correlations of MR parameters within each patient the values of MR parameters were averaged for each patient prior to the application of paired t-test. Correlations between MR parameters and GS were evaluated by averaging Spearman's correlation coefficients calculated for individual patients. Significance of the correlation between MR parameters and GS was evaluated with the application of one sample t-test. $P<0.05$ was considered statistically significant. Area under the receiver operating characteristic (ROC) Curve (AUC)

was calculated by ROC analysis [21] of individual and combined MR parameters, performed in PZ, TZ, and the entire prostate. ROC analyses were performed based on logistic generalized linear mixed effect models (GLMMs). Correlation within each patient was incorporated by having a random intercept in the model with the grouping factor for the random intercept being each patient. Multi-parametric ROC analyses were performed by using logistic GLMM, while only parameters that contributed significantly to the model, and also minimized Akaike information criterion (AIC) and Bayesian information criterion (BIC), were used.

Results

Clinical data (i.e., age, PSA levels, prostate volume, Gleason score distribution, and pathologic stage) for the 18 patients who participated in this study are summarized in Table 1.

Representative maps of MR parameters are shown in Figure 2, and their mean values and ranges are provided in Table 2.

Results of the paired t-test indicate that the average values of gmT_2, A_{short}, A_{long}, and LWF are significantly different between malignant and non-malignant tissue in the entire prostate. Results of paired t-test in PZ showed that all MRI parameters except for $T_{2\text{-}long}$ have significantly different average values between malignant and non-malignant tissue. Paired t-test could not be conducted in TZ due to the insufficient number of patients with tumors in TZ.

Average Spearman's rank correlation coefficients between MR parameters and GS, and the results of t-test in PZ are presented in Table 3. T-test could not be conducted in TZ due to the insufficient number of patients with tumors in TZ. LWF showed the strongest correlation with Spearman's coefficient values of -0.78 ± 0.01.

The values of AUCs calculated from ROC analysis are summarized in Table 4. LWF had the highest AUC in PZ (0.97), TZ (0.98), and the A_{short} had the highest AUC in the entire gland (0.82).

Multi-parametric ROC analysis in PZ showed slightly increased AUC (0.98 vs. 0.97), with only gmT_2 and $T_{2\text{-}short}$ contributing significantly to the logistic regression model (Regression coefficients: -9 ± 2 ($P<0.0001$), 6 ± 1 ($P<0.0001$), respectively). Multi-parametric ROC analysis could not be performed in TZ, since the only parameter that contributed significantly to the model was LWF. In the entire prostate, multi-parametric ROC analysis again showed increased AUC (0.86 vs. 0.82), with gmT_2, $T_{2\text{-}short}$, A_{short}, and N_{comp} contributing significantly to the model (Regression coefficients: -5.4 ± 0.9 ($P<0.0001$), 4.4 ± 0.7 ($P=0.0002$), 0.7 ± 0.2 ($P=0.002$), 0.9 ± 0.2 ($P=0.0001$), respectively).

Discussion

The results of this pilot study demonstrate the feasibility of multi-exponential T_2 mapping for prostate cancer (PCa) diagnosis. Although, multi-component T_2 in prostate has been

shown before [6, 7, 8, 9, 10] only one recent study investigated the application of this technique for cancer diagnosis [10]; however, no direct correlation between MRI and histology has been published. In our study, we validated MR measurements with whole-mount histology, and performed statistical analysis to assess the accuracy of this technique in the detection and grading of PCa. In addition, we used a regularized NNLS algorithm, which provides an unbiased assessment of the number of T_2 components and the increased accuracy of T_2 estimation in the presence of noise [22]. We also introduced a new parameter: the fractional volume of the long T_2 component, or Luminal Water Fraction (LWF), which outperformed all the other MRI parameters in detecting and grading PCa. In addition, LWF represents a morphological feature of the tissue, i.e. the percentage of the luminal space, and thus lends itself to a physiological interpretation more easily than most other MRI parameters.

The mean and range of LWF values measured in non-malignant PZ in this study is in good agreement with the published values of the percentage area of lumen in normal prostatic tissue (0.24 (0.09–0.45) vs. 29.6% (15.9%–43.9%)) [23], suggesting that LWF can be a good measure of luminal space in prostate. This is strongly supported by our recent study [24], which showed a significant correlation between LWF and the histological measure of luminal space. The mean and range of gmT_2, $T_{2\text{-short}}$, and $T_{2\text{-long}}$ also corresponds well to the previously published values [7, 8].

Our results showed lower gmT_2, A_{long}, and LWF values in tumors and in normal dense stroma than in the non-malignant glandular tissue. In general, in PCa, some of the loose stroma that fills the area between ducts and acini is replaced by densely packed malignant epithelial cells, decreasing the percentage of lumen. Therefore it is not surprising to see a decrease in A_{long} and LWF in these cancers.

There was no significant difference in N_{comp}, $T_{2\text{-long}}$ and $T_{2\text{-short}}$ between non-malignant and malignant tissues. This is likely because T_2 will depend not only on the size of the water compartment, but also on its shape, or more accurately, its surface to volume ratio [25, 26]. Thus one would not necessarily expect significant differences of $T_{2\text{-long}}$ between tumor and normal tissue. We observed fairly large variability in $T_{2\text{-long}}$, most likely related to the variability of individual glands' surface to volume ratio.

Average values of N_{comp} were lower in tumor and normal dense stroma than in the non-malignant glandular tissue in PZ; thus N_{comp} can be considered an indicator of how glandular the tissue is. Generally, in higher grade tumors the lumen shrinks significantly and more T_2-decay curves become mono-exponential, thus decreasing the average N_{comp} values. Therefore one would expect N_{comp} to be significantly different between normal glandular and higher grade cancerous tissue. Since the analysis of the entire prostate included normal stroma ($N_{comp} \approx 1$) and lower grade tumors ($N_{comp} \approx 2$), it is not surprising to see no significant difference in N_{comp} between non-malignant and malignant tissue.

Our results demonstrate significant correlation between LWF and GS in both PZ and TZ. The decreasing LWF with increasing GS is aligned with the published values for percentage of lumen in normal tissue and in tumors of Gleason scores 6 and 7 [23]. Such dependence

underscores the role of LWF as a morphologic parameter that correlates with known histologic features. It is recognized that Gleason pattern 4 carcinoma has poorly formed fused glands and is often characterized by a dense cribriform pattern. Gleason pattern 4 carcinoma has significant collapse and loss of luminal formation, contrasting with Gleason 3 carcinoma that has malignant glands with open lumina [27]. Thus one may expect lowered LWF with this loss of luminal space and increased cell density.

LWF had much higher AUC in PZ and TZ than in the entire prostate. This is likely because, with regards to the luminal space, the normal dense stroma mimic the tumors in PZ and TZ. Our results show that combining N_{comp} with any other MR parameter improves specificity and AUC within the entire prostate; this suggests that N_{comp} can potentially be useful in tissue classification algorithms.

The main limitation of this pilot study was the relatively low number of patients. Also, the range of Gleason Score in this study was limited, with 35 lesions of GS=6, 13 GS=7, 1 GS=8, 6 GS=9 and none with GS=10. Another limitation of this study includes lack of distinction between normal gland, BPH, and prostatitis. Also, a patient selection process was biased, as the recruited patients were selected from those who were scheduled for retropubic prostatectomy, indicating that the sampled lesions were weighted toward more advanced tumors.

Areas of future research with this technique include expanding this study with a larger number of patients and wider range of Gleason Scores with larger numbers in each category to access the accuracy of this technique. Comparison of this technique with the current PIRADs version 2 protocol [28] would also be useful in determining its clinical utility. Also combining it with current PIRADS version 2 protocol to determine if it further increases accuracy and its incremental benefit should be investigated.

In conclusion, the results of this pilot study demonstrate the feasibility of Luminal Water Imaging for diagnosis and grading of prostate cancer. Four MR parameters showed significant differences between malignant and non-malignant tissue in the prostate. LWF showed very high accuracy in detection of prostatic tumors, and a strong correlation with Gleason score. N_{comp} was found to increase the specificity of this technique in the entire prostate. Our preliminary results have shown that the proposed MRI technique can be applied for both the detection and grading of prostate cancer with high accuracy. To accurately assess the suitability of this technique for clinical application, a prospective study with much larger number of patients and broader range of tumor grades, and a comparison to the current clinical PIRADs version 2 protocol should be done.

Acknowledgments

This study was supported by the Canadian Institutes of Health Research (MOP-115052).

The authors thank Dr. Martin Gleave, and Dr. Alan So from Vancouver General Hospital for their invaluable cooperation in patient recruitment, Margaret Luk from Vancouver General Hospital for all her support in preparation of whole-mount histology sections, Dr. Ladan Fazli and Janet Liew from Vancouver Prostate Centre for producing the whole mount prostate slides, and the supportive staff of UBC MRI Research Centre, especially Alex Mazur and Laura Barlow, for their effort in MRI data acquisition. The authors also thank Tingting Yu from UBC department of statistics for her statistical advices as well as performing part of the statistical analysis.

Funding:

This study was supported by the Canadian Institutes of Health Research (MOP-115052).

References

1. Mackay A, Kenneth W, Julian A, Li D, Paty D, Graeb D. In Vivo Visualization of Myelin Water in Brain by Magnetic. Resonance. Magn Reson Med. 1994; 31(6):673–7. [PubMed: 8057820]
2. Kijowski R, Blankenbaker DG, Munoz Del Rio A, Baer GS, Graf BK. Evaluation of the articular cartilage of the knee joint: value of adding a T2 mapping sequence to a routine MR imaging protocol. Radiology. 2013; 267(2):503–13. [PubMed: 23297335]
3. Nguyen K, Sarkar A, Jain AK. Prostate Cancer Grading: Use of Graph Cut and Spatial Arrangement of Nuclei. IEEE Transactions on Medical Imaging. 2014; 33(12):2254–70. [PubMed: 25029379]
4. McNeal JE. Normal histology of the prostate. Am J Surg Pathol. 1988; 12(8):619–33. [PubMed: 2456702]
5. Hammerich, KH., Ayala, GE., Wheeler, TM. Anatomy of the prostate gland and surgical pathology of prostate cancer. In: Hrical, H., Scardino, PT., editors. Prostate Cancer. Cambridge University Press; 2008. p. 1-14.
6. Kjaer L, Thomsen C, Iversen P, Henriksen O. In Vivo Estimation of Relaxation Processes in Benign Hyperplasia and Carcinoma of the Prostate Gland by Magnetic Resonance Imaging. Magnetic Resonance Imaging. 1987; 5(1):23–30. [PubMed: 2438532]
7. Storås TH, Gjesdal KI, Gadmar ØB, Geitung JT, Kløw NE. Prostate Magnetic Resonance Imaging: Multiexponential T2 Decay in Prostate Tissue. J Magn Reson Imaging. 2008; 28(5):1166–72. [PubMed: 18972358]
8. Storås TH, Gjesdal KI, Gadmar ØB, Geitung JT, Kløw NE. Three-dimensional Balanced Steady State Free Precession Imaging of the Prostate: Flip Angle Dependency of the Signal Based on a Two Component T2-decay Model. J Magn Reson Imaging. 2010; 31(5):1124–31. [PubMed: 20432347]
9. Gilani N, Rosenkrantz AB2, Malcolm P, Johnson G. Minimization of Errors in Biexponential T 2 Measurements of the Prostate. J Magn Reson Imaging. 2015; 42(4):1072–7. [PubMed: 25704897]
10. Wang, S., Agarwal, H., Karczmar, GS., Oto, A. Two-compartment T2 Decay for Prostate Cancer Diagnosis. Proceedings of the 23rd Annual Meeting of ISMRM; Toronto, Ontarion, Canada. 2015; Abstract 944
11. Drew B, Jones EC, Reinsberg S, Yung AC, Goldenberg SL, Kozlowski P. Device for sectioning prostatectomy specimens to facilitate comparison between histology and in vivo MRI. Journal of Magnetic Resonance Imaging. 2010; 32(4):992–996. [PubMed: 20882632]
12. Zhang, J., Vavasour, I., Kolind, S., Baumeister, B., Rauscher, A., MacKay, AL. Advanced Myelin Water Imaging Techniques for Rapid Data Acquisition and Long T2 Component Measurements. Proceedings of the 23rd Annual Meeting of ISMRM; Toronto, Ontario, Canada. 2015; Abstract 824
13. Uribe CF, Jones EC, Chang SD, Goldenberg SL, Reinsberg SA, Kozlowski P. In vivo 3T and ex vivo 7T diffusion tensor imaging of prostate cancer: Correlation with histology. Magn Reson Imaging. 2015; 33(5):577–83. [PubMed: 25721995]
14. Bjarnason TA, Mitchell JR. Analyze NNLS: magnetic resonance multiexponential decay image analysis. J Magn Reson. 2010; 206(2):200–4. [PubMed: 20688549]
15. Prasloski T, Mädler B, Xiang QS, MacKay A, Jones C. Applications of Stimulated Echo Correction to Multicomponent T2 Analysis. Magn Reson Med. 2012; 67(6):1803–14. [PubMed: 22012743]
16. Whittall KP, MacKay AL, Graeb DA, Nugent RA, Li DK, Paty DW. In vivo measurement of T2 distributions and water contents in normal human brain. Magn Reson Med. 1997; 37(1):34–43. [PubMed: 8978630]
17. Laule C, Kozlowski P, Leung E, Li DK, Mackay AL, Moore GR. Myelin water imaging of multiple sclerosis at 7 T: correlations with histopathology. Neuroimage. 2008; 40(4):1575–80. [PubMed: 18321730]

18. Dragulescu AA, Apache XML, Beans POI, Maintainer Dragulescu AA. Package 'xlsxjars'. 2014
19. Bates D, Maechler M, Bolker B, Walker S. Fitting Linear Mixed-Effects Models Using lme4. Journal of Statistical Software. 2015; 67(1):1–48.
20. Robin X, Turk N, Hainard A, et al. pROC: an open-source package for R and S+ to analyze and compare ROC curves. BMC Bioinformatics. 2011; 12:77. [PubMed: 21414208]
21. Obuchowski NA. Receiver operating characteristic curves and their use in radiology. Radiology. 2003; 229(2):3–8. [PubMed: 14519861]
22. MacKay AL, Laule C, Vavasour I, Bjarnason T, Kolind S, Mädler B. Insights into brain microstructure from the T2 distribution. Magnetic Resonance Imaging. 2006; 24(4):515–25. [PubMed: 16677958]
23. Langer DL, van der Kwast TH, Evans AJ, et al. Prostate tissue composition and MR measurements: investigating the relationships between ADC, T2, K(trans), v(e), and corresponding histologic features. Radiology. 2010; 255(2):485–94. [PubMed: 20413761]
24. Sabouri, S., Fazli, L., Chang, S., et al. MR measurements of luminal water in prostate gland. Proceedings of the 24thd Annual Meeting of ISMRM; Singapore. 2016; Abstract 2487
25. Menon RS, MacKay AL, Hailey JRT, Bloom M, Burgess AE, Swanson JS. An NMR determination of the physiological water distribution in wood during drying. Journal of Applied Polymer Sciences. 1987; 33(4):1141–1155.
26. Halperin WP, Jehng JY, Song YQ. Application of spin-spin relaxation to measurement of surface area and pore size distributions in a hydrating cement paste. Magn Reson Imaging. 1994; 12(2): 169–173. [PubMed: 8170292]
27. Gleason DF. Histologic grading of prostate cancer: a perspective. Hum Pathol. 1992; 23(3):273–9. [PubMed: 1555838]
28. PI-RADS, Prostate Imaging – Reporting and Data System, Version2. American College of Radiology Web site. http://www.acr.org/~/media/ACR/Documents/PDF/QualitySafety/Resources/PIRADS/PIRADS%20V2.pdf. Published 2015

Advances in Knowledge

1. Average values of four magnetic resonance imaging (MRI) parameters: geometric mean T_2 (gmT_2), A_{short}, A_{long}, and luminal water fraction (LWF) showed significant differences between malignant and non-malignant tissue in the prostate.
2. LWF, which was defined and used for the first time in this study, showed a strong correlation with Gleason score (-0.78 ± 0.11, $p < 0.001$ in peripheral zone (PZ)), and showed high area under the ROC curve (AUC) (0.97 in PZ and 0.98 in TZ) in detection of prostatic tumors.

Implications for Patient Care

1. The proposed magnetic resonance imaging technique can potentially be applied to aid in detection of cancerous tissue and grading of prostate cancer.

Summary

The results of this pilot study demonstrate the feasibility of Luminal Water Imaging for diagnosis and grading of prostate cancer.

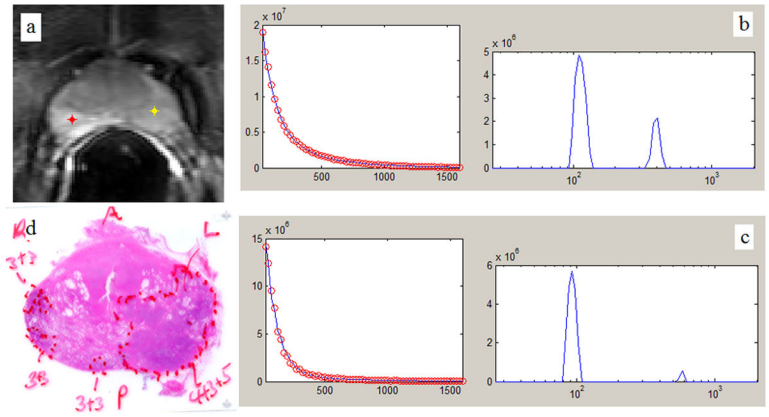

Figure 1.

a: 1st echo T_2W image of an axial cross section from a middle level of a prostate gland. b: Non-Negative Least Squares (NNLS) fitting of the multi-exponential T_2 decay curve (left-hand side) generated from the pixel in non-malignant PZ (red marker in a.), and its correspondent T_2 distribution (right-hand side). c: NNLS fitting of the multi-exponential T_2 decay curve (left-hand side) generated from the pixel in malignant PZ (yellow marker in a.), and its correspondent T_2 distribution (right-hand side).d: histology whole-mount section of the same slice.

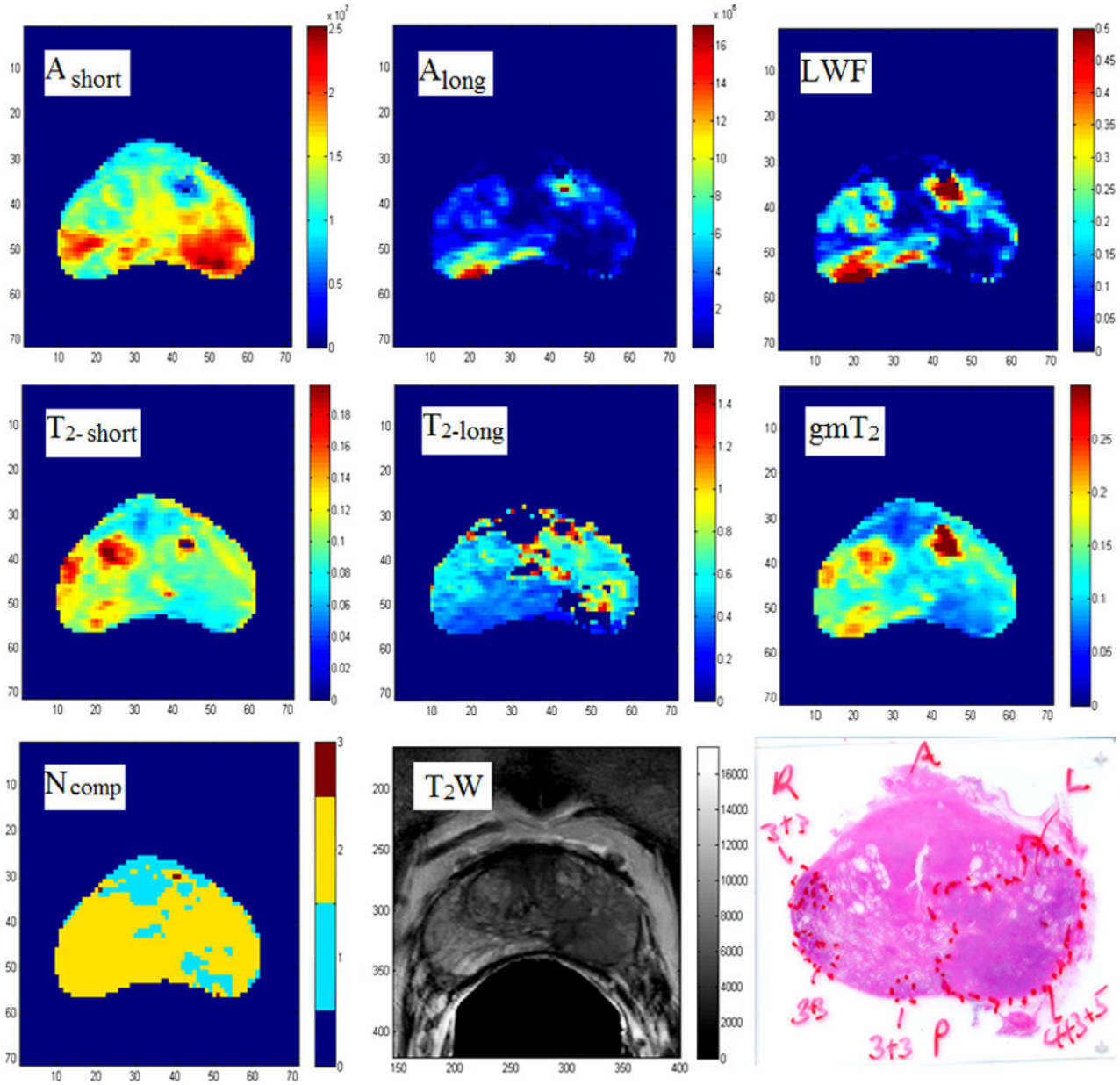

Figure 2.

Representative maps of MR parameters, T_2-weighted image, and histology whole-mount section of the same slice. Scale bar of gm T_2, $T_{2\text{-short}}$, and $T_{2\text{-long}}$ images are in 's'. Zero pixels on the $T_{2\text{-long}}$ map indicate mono-exponential decay.

Table 1

Clinical data of 18 patients participating in the study.

Patient	Age (y)	PSA level (ng/mL)	Prostate volume (cc)	Lesion characteristics				Pathologic tumor stage
				Size (cc)	Gleason grade	Location	Total number of ROIs per lesion (from different slices)	
P01	65	13.1	32.3	5.8	4+3	PZ	7	pT3a
P02	65	4.6	67.5	0.1	3+4	TZ	1	pT2c
				0.1	3+3	TZ	1	
				2×0.1	3+3	PZ	2	
P03	67	8	94.7	0.7	3+3	PZ	4	pT2c
				2×0.2	3+3	PZ	4	
				0.5	3+3	TZ	2	
				0.3	3+3	TZ	3	
P04	62	6.5	31.0	3.2	4+3	PZ	6	pT3a
				0.2	4+3	PZ	2	
				0.1	3+3	PZ	1	
				0.5	3+3	TZ	4	
P05	80	7.2	128.3	0.1	3+3	PZ	2	pT2a
P06	64	7.6	32.3	7.5	4+3	PZ	8	pT3a
				0.9	3+3	PZ	4	
P07	75	18.2	41.1	3.3	4+3	PZ	5	pT2c
				1.5	3+3	PZ	4	
				3×0.1	3+3	PZ	3	
				4×0.1	3+3	TZ	4	
				5×0.2	3+3	TZ	9	
P08	62	13.5	23.4	6.8	4+5	PZ	8	pT3b
				0.3	3+3	PZ	2	
				3×0.1	3+3	PZ	3	
P09	75	7.9	31.0	0.9	4+5	PZ	2	pT3a
				0.5	4+3	PZ	1	
				0.3	3+3	TZ	2	
P10	69	18.4	39.5	6.2	4+5	TZ	5	pT3a
P11	66	7.4	32.5	1.0	3+4	PZ	1	pT3a

Patient	Age (y)	PSA level (ng/mL)	Prostate volume (cc)	Lesion characteristics				Pathologic tumor stage
				Size (cc)	Gleason grade	Location	Total number of ROIs per lesion (from different slices)	
P12	67	6	17.7	1.3	3+4	PZ	3	pT3a
				0.1	3+3	PZ	1	
				0.6	3+3	TZ	2	
P13	58	6.7	31.4	6.1	3+4	PZ	8	pT3a
				3.3	3+4	PZ	5	
P14	58	12	20.2	3.9	3+4	PZ	5	pT3a
				0.1	3+3	PZ	1	
				0.2	3+3	TZ	1	
P15	66	31.6	44.9	6.6	4+3	PZ	9	pT3a
P16	75	8.5	36.6	3.2	4+5	PZ	4	pT3a
				0.4	4+5	PZ	2	
				0.1	3+3	PZ	1	
P17	63	51	26.4	9.5	4+5	PZ	6	pT3b
P18	62	13.3	33.3	2.1	4+4	PZ	4	pT3a

Table 2

MR measurements in malignant and non-malignant tissues of different regions

		$T_{2\text{-short}}$ (ms)	$T_{2\text{-long}}$ (ms)	gmT_2[a] (ms)	LWF[b]	A_{short} ($\times 10^5$)	A_{long} ($\times 10^5$)	N_{comp}
Non-malignant PZ[c]	Mean Range	90±26 [52–150]	545±115 [300–887]	138±46 [68–298]	0.24±0.09 [0.09–0.45]	165±51 [90–350]	52±23 [16–116]	2.09±0.22 [1.4–2.67]
Malignant PZ	Mean Range	81±21* [44–157]	548±188 [207–1408]	94±27* [46–187]	0.10±0.05* [0–0.3]	188±46* [89–303]	22±12* [0.2–73]	1.81±0.28* [1.06–2.52]
Non-malignant TZ[d]	Mean Range	104±38 [56–202]	548±183 [281–914]	138±49 [65–276]	0.20±0.08 [0.06–0.43]	168±40 [104–250]	41±21 [13–97]	1.94±0.19 [1.52–2.52]
Malignant TZ	Mean Range	90±22 [37–124]	609±270 [372–1035]	101±30 [39–158]	0.08±0.05 [0–0.15]	165±36 [118–292]	15±11 [0–34]	1.66±0.37 [1–2]
Normal AFM	Mean Range	57±12 [31–84]	639±281 [219–1323]	58±14 [28–97]	0.06±0.05 [0–0.21]	154±30 [95–262]	9±9 [0–40]	1.39±0.25 [1–1.92]
Normal PFMS	Mean Range	75±22 [37–115]	639±271 [258–1078]	77±22 [38–116]	0.04±0.03 [0–0.11]	165±31 [107–228]	8±5 [0–21]	1.39±0.27 [1–1.96]
Entire prostate	Mean Range	84±28 [31–202]	569±204 [207–1408]	106±45 [28–298]	0.14±0.10 [0–0.45]	172±46 [89–350]	29±23[0–116]	1.80±0.36 [1–2.67]

[a] gm T_2: geometric mean T_2

[b] LWF: luminal water fraction

[c] PZ: peripheral zone

[d] TZ: transition zone.

* Malignant PZ significantly different than non-malignant PZ ($P<0.05$) based on paired t-test. Paired t-test could not be conducted in TZ due to the insufficient number of patients with tumors in TZ.

Table 3

Statistical correlations of MRI multi-exponential decay parameters with Gleason score in PZ; data from 17 patients were included.

		$T_{2\text{-short}}$	$T_{2\text{-long}}$	gmT_2	LWF	A_{short}	A_{long}	N_{comp}
PZ	Average Spearman's coefficient of rank correlation (ρ) ± standard deviation	−0.34±0.49	0.17±0.45	−0.66±0.34	−0.78±0.11	0.38±0.48	−0.76±0.11	−0.56±0.30
	95% Confidence Interval for ρ	−0.596 to −0.093	−0.065 to 0.399	−0.832 to −0.485	−0.834 to −0.726	0.133 to 0.628	−0.814 to −0.697	−0.716 to −0.408
	Significance level	P = 0.010	P = 0.146	P < 0.0001	P < 0.0001	P = 0.005	P < 0.0001	P < 0.0001
	Test statistic t	2.902	1.525	8.046	30.500	3.263	27.349	7.736

Table 4

ROC analysis measures for MRI parameters in PZ, TZ, and entire prostate.

		$T_{2\text{-short}}$	$T_{2\text{-long}}$	gmT_2	LWF	A_{short}	A_{long}	N_{comp}
PZ	Area under the ROC curve (AUC)	0.84±0.05	0.76±0.06	0.96±0.03	0.97±0.02	0.85±0.05	0.97±0.02	0.88±0.05
TZ	Area under the ROC curve (AUC)	0.97±0.03	0.89±0.07	0.98±0.02	0.98±0.02	0.94±0.05	0.95±0.04	0.92±0.05
Entire prostate	Area under the ROC curve (AUC)	0.70±0.05	0.69±0.05	0.72±0.05	0.74±0.05	0.82±0.04	0.71±0.05	0.69±0.05